NASA TECHNICAL MEMORANDUM
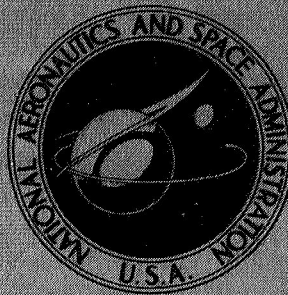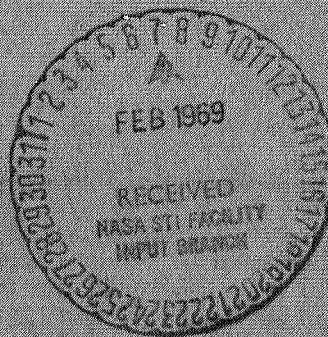
NASA TM X-1727

CASE FILE
COPY

INVESTIGATION OF FLOW RANGE
AND STABILITY OF THREE
INDUCER-IMPELLER PUMP COMBINATIONS
OPERATING IN LIQUID HYDROGEN

by Donald C. Urasek

Lewis Research Center
Cleveland, Ohio

INVESTIGATION OF FLOW RANGE AND STABILITY OF THREE

INDUCER-IMPELLER PUMP COMBINATIONS

OPERATING IN LIQUID HYDROGEN

By Donald C. Urasek

Lewis Research Center
Cleveland, Ohio

NATIONAL AERONAUTICS AND SPACE ADMINISTRATION

ABSTRACT

The effect of inducer-impeller matching on flow range and stability was studied by running three variable lead inducers in combination with a centrifugal impeller. The three inducers were designed for flows of 0.80, 1.00, and 1.20 of impeller design flow. The low flow limit imposed by unstable flow was essentially independent of inducer-impeller matching, whereas the high flow limit imposed by cavitation was improved when the inducer was designed for a higher flow rate than that of the impeller.

INVESTIGATION OF FLOW RANGE AND STABILITY OF THREE

INDUCER-IMPELLER PUMP COMBINATIONS

OPERATING IN LIQUID HYDROGEN

by Donald C. Urasek

Lewis Research Center

SUMMARY

The useful flow range of a pump is bounded by the high flow limit imposed by cavitation and a low flow limit imposed by unstable flow. The effect of inducer-impeller matching on flow range and stability was studied by running three variable lead inducers in combination with a centrifugal impeller. The three inducers were designed for flows of 0.80, 1.00, and 1.20 of impeller design flow. The unstable flow conditions was essentially independent of inducer-impeller matching. The cavitation performance of the pump was improved when the inducer was designed for a higher flow rate than that of the impeller.

INTRODUCTION

A broad flow range is required for some rocket engine propellant pumps to accommodate engine start transients and variable thrust. The useful flow range of a pump is bounded by its high flow limit imposed by cavitation and its low flow limit imposed by unstable flow.

In general, the propellant pumps for rocket engines are designed with an inducer followed by one or more high-pressure stages. The inducer is designed to operate at low inlet pressure under cavitating conditions, which thereby permits a lower propellant tank pressure. The inducer provides a sufficient pressure rise to suppress cavitation in the high-pressure stages. The high flow limit of a pump, which is controlled by cavitation, is thus extended by the inducer. However, to increase the overall flow range of the pump, consideration should also be given to the low flow limit. Increasing the inducer design flow rate results in increased blade loading at a given reduced flow rate. High blade loading may result in flow separation leading to unstable operation of

the inducer or a failure to provide the proper flow conditions into the pressure stage. The latter condition may, in turn, result in unstable operation of the pressure stage. Also, high inducer blade loading may result in increased total pressure losses in the inducer and/or the pressure stage. For a centrifugal pump with radial blades, the pressure rise is essentially independent of flow, being altered only by slip (flow deviation at impeller exit) and losses. Thus, higher losses in the inducer - centrifugal-pump system may cause the slope of the head-flow curve to become positive at a higher flow, resulting in a pumping system that is susceptible to system surge (ref. 1). The useful flow limit of a pump may be affected by the flow matching between the inducer and pressure stage.

The effects of inducer design flow on the low flow limit of a pump were investigated with three inducers, designed for three different weight flows, that were tested in combination with one radial bladed centrifugal impeller. The three inducers were designed to produce a given pressure rise at flow rates of 0.80, 1.00, and 1.20 of the impeller design flow rate. The performance of the pump with each of the three inducers was evaluated in liquid hydrogen over three operating speeds. In each test, the flow was reduced from the maximum obtainable to the point where pump operation became unstable. Data were generated over a range of values of net positive suction pressure. The tests were conducted at the NASA Lewis Research Center, Plum Brook Station.

PUMP DESIGN

The overall design flow coefficient and head coefficient were arbitrarily selected to be 0.074 and 0.72, respectively. At a rotational speed of 30 000 rpm, the design flow rate was 550 gallons per minute (0.0347 cu m/sec) and the pressure rise was 244 psi (168 N/cm^2). At this rotational speed, the design net positive suction pressure was selected as 1.25 psi (0.86 N/cm^2). The resulting suction specific speed at the design flow rate was 43 650.

Inducer Design

Three helical bladed inducers were designed for the following conditions: flow ratios of 0.80, 1.00, and 1.20 of nominal design flow (they are referred to as the 0.80-, 1.00-, and 1.20-inducers); an inlet flow coefficient of 0.074; and a tip blade angle of 82°, as measured from the axial direction. This flow coefficient and blade angle resulted in an incidence angle of about 3.75° at the blade tip. This combination of flow coefficient and incidence angle selected was based on the optimization method presented in references 2 and 3, which indicates that an inducer designed for these conditions is theoretically

2

capable of meeting the nominal suction specific speed of 43 650. In practice, suction specific speeds in excess of 30 000 have been difficult to achieve with inducers operating in cold water (ref. 2). However, additional benefits in cavitation performance have been demonstrated for inducers operating in liquid hydrogen (ref. 4). The flow passage area was reduced across each of the inducers to match the inducer exit area with the impeller inlet. The hub and tip contours of the inducers were tapered, as shown in figure 1. The flow area was adjusted to satisfy the design flow of each inducer and the selected design flow coefficient. The change in passage height between the inducer inlet and exit, as indicated in figure 1, permitted the use of a low flow coefficient at the inducer inlet to
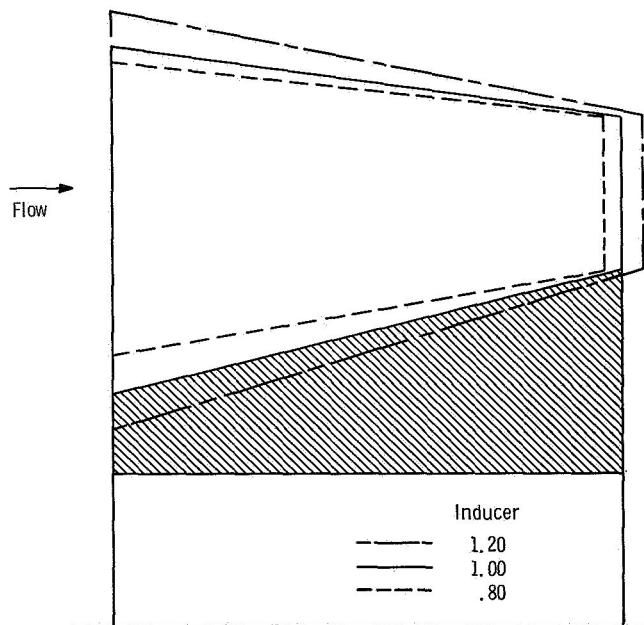

Flow

Inducer

—————— 1.20
———————— 1.00
— — — — .80

Figure 1. – Comparison of geometric flow passages of three test inducers.

obtain good cavitation performance, and at the same time, a high flow coefficient at the impeller inlet. A helical blade shape was selected for the inducer. All three inducers were designed with two blades and a tip solidity of 2. The inducers were loaded at the leading edge only as a result of incidence. The resulting head coefficient for all three inducers was 0.22, based on the inducer exit tip diameter. Because of the change in axial velocity, due to reduction in flow area, it was necessary to vary the lead of the helix to maintain a constant total head through the inducer passage. Other pertinent design information is given in table I. The three inducers are shown in the photograph of figure 2.
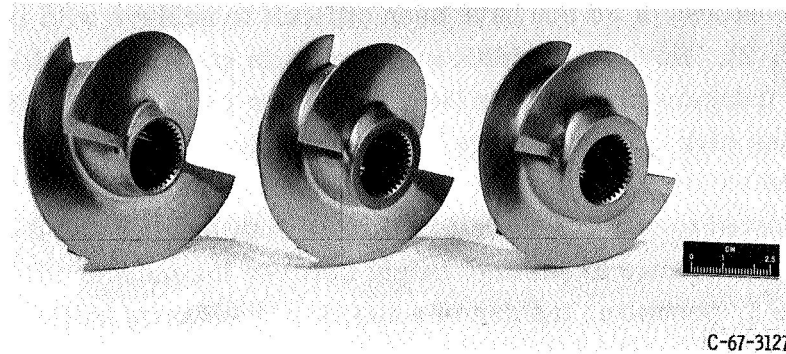
1.20   1.00   0.80

Flow ratio

Figure 2. - Test inducers.

Centrifugal Impeller Design

A slip factor of 0.90 was employed in the impeller design calculations along with an assumed overall efficiency of 0.80, which resulted in a head coefficient of 0.72 for the pump. An impeller inlet hub-tip radius ratio of 0.70 was selected. The blade angle at the impeller inlet hub and tip was set equal to the outlet angles at the hub and tip of the 1.00-inducer. For this inducer-impeller configuration, then, the impeller incidence angle for the impeller and the inducer deviation were equal. The outlet blade angle was set equal to zero. The impeller blade mean surface was defined by the following equation:

$$\theta = 1.784 \, \alpha^{1.3} - 2.656 \, \alpha \tag{1}$$

The angles θ and α are shown in figure 3 and defined in appendix A. The constants in the equation were selected to provide the desired inlet and outlet flow angles and to give a nearly linear distribution in blade angle through the impeller. A circular arc was arbitrarily selected for the hub contour. The center of rotation of the lines that define the mean blade shape (point A, fig. 3) was located at the center of radii of the hub contour, and, thus, the meanline elements of the blade are perpendicular to the hub surface. With the inlet and outlet impeller geometry established and the blade shape and hub contour selected, the stream filament method (ref. 5) was employed in calculating the flow velocities in the hub-to-shroud plane. A linear variation in static pressure from blade to blade was assumed to determine the flow velocities along the blade surfaces. The shroud contour, the number of both the full and partial blades, and the location of the partial

4
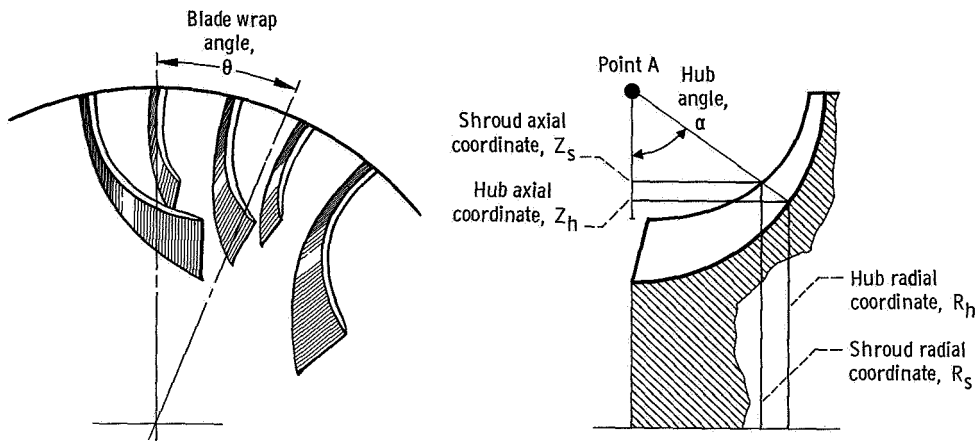
Figure 3. - Cylindrical coordinate system for radial bladed centrifugal impeller.

CD-10114-01

blades were adjusted to obtain the desired velocity distribution in both the meridional hub-to-shroud and the blade-to-blade planes. In particular, indicated negative velocities were avoided along the pressure surfaces of the blade by proper adjustment in flow area and an addition of splitter (partial) blades. The final design resulted in 12 main blades with 12 splitters starting at a distance of 50.5 percent of the main blade length and 24 additional splitters starting at 68.5 percent of the main blade length for a total of 48 blades at the impeller discharge. The final impeller configuration showing the hub and shroud contour and the blade leading edges is shown in figure 4. A photograph of the 1.0-inducer-impeller combination is presented in figure 5. The two rotors were separated by a 1-inch (2.54-cm) spacer to allow for insertion of instrumentation behind the inducer. The ratio of the calculated local relative velocity to the inlet tip relative velocity is shown as a function of blade length in figure 6. These velocities were calculated by using the design flow rate and the resulting flow distribution from the 1.00-inducer. For stream surfaces along both the hub and the shroud, the velocity distribution is given for the pressure, midchannel, and suction surfaces. The theoretical solution was connected with straight lines, and no attempt was made to fair in a curve between the points. The velocity distribution shows the relative velocity along the pressure surface near the hub approaching zero, which indicates a potential eddy condition at a reduced flow. A blade blockage allowance of 32 percent of the outlet theoretical blade height, varying linearly to zero at the blade inlet, was used to establish the actual impeller shroud. Cylindrical coordinates for the final hub and shroud configurations are listed in table II (see fig. 3 for reference).
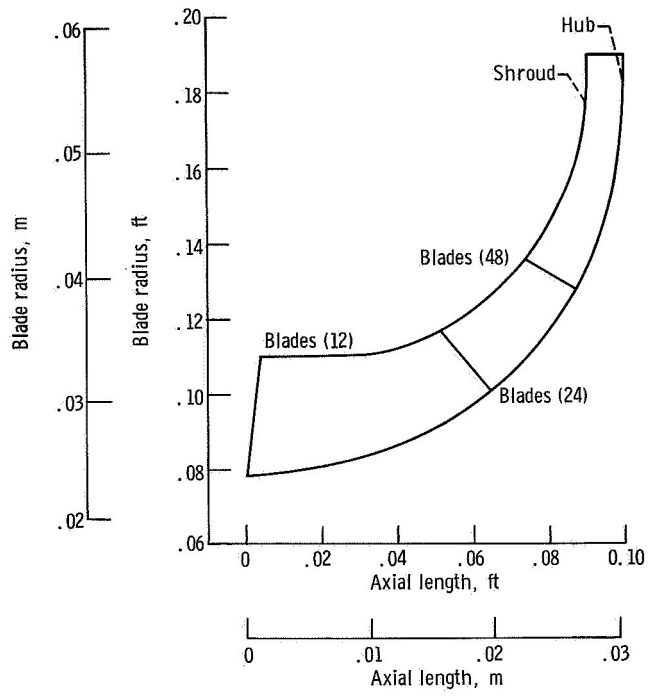
Figure 4. - Impeller blade contour.
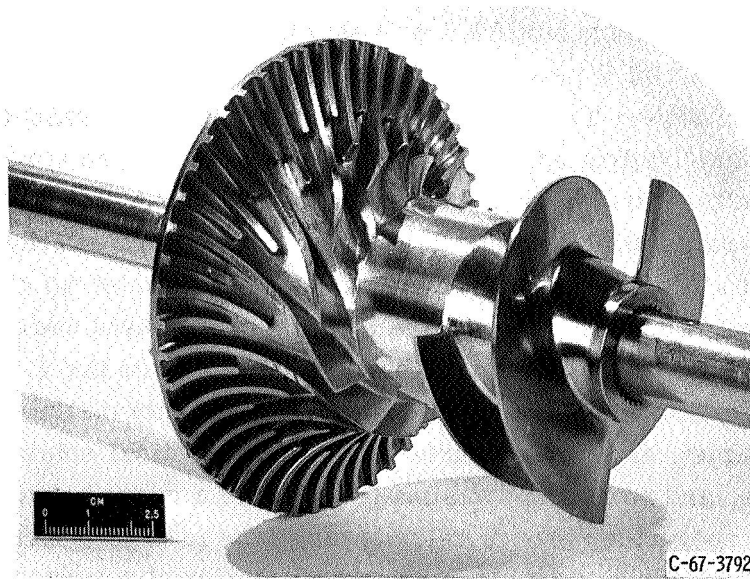
Figure 5. - 1.00-Inducer-impeller configuration.

6

Relative velocity ratio, $W/W_{i,t}$

1.2

1.0 — Suction surface

.8 — Midchannel

Pressure surface

.6 — Suction surface

.4 — Midchannel

Pressure surface

Shroud
Hub

.2

0   .04   .08   .12   .16   .20   .24
Blade length, ft

0   .015   .030   .045   .060
Blade length, m
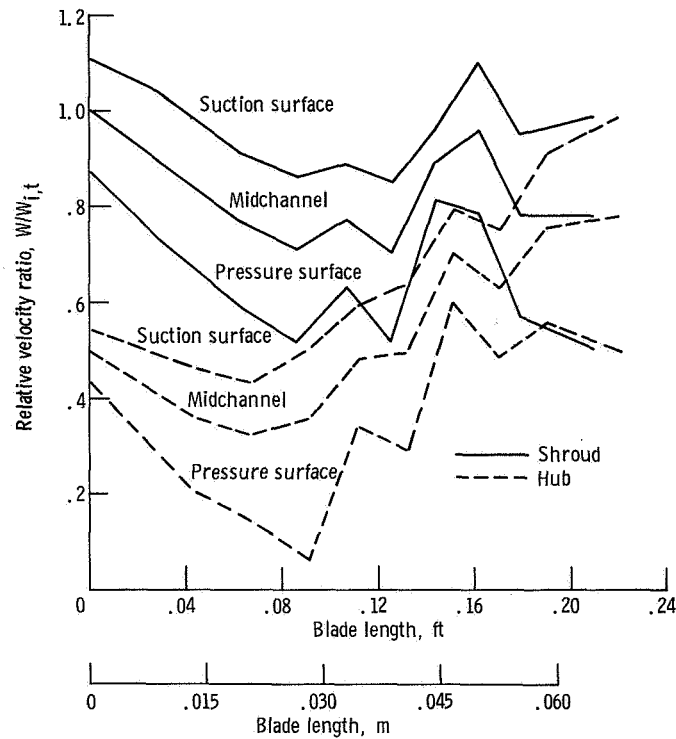
Figure 6. – Theoretical relative velocity ratio in impeller blade passage at design flow with 1.00-inducer. Rotative speed, 30 000 rpm.

Diffuser and Scroll Design

A short radial vaneless diffuser of constant width was incorporated immediately downstream of the impeller; the radial length was approximately 0.5 inch (1.27 cm). Downstream of the vaneless diffuser, a teardrop-shaped scroll was employed. The area distribution was circumferentially sized to maintain essentially a constant velocity. At the scroll tongue, the teardrop shape was faired into a conical diffuser with a 6° cone angle.

APPARATUS AND PROCEDURE

Test Pump and Drive Turbine

The pump was driven by a gaseous-hydrogen three-stage axial-flow turbine. A cutaway view of the pump and turbine assembly is shown in figure 7. The pump shaft was supported by two liquid-hydrogen-cooled angular contact ball bearings. Axial thrust

7
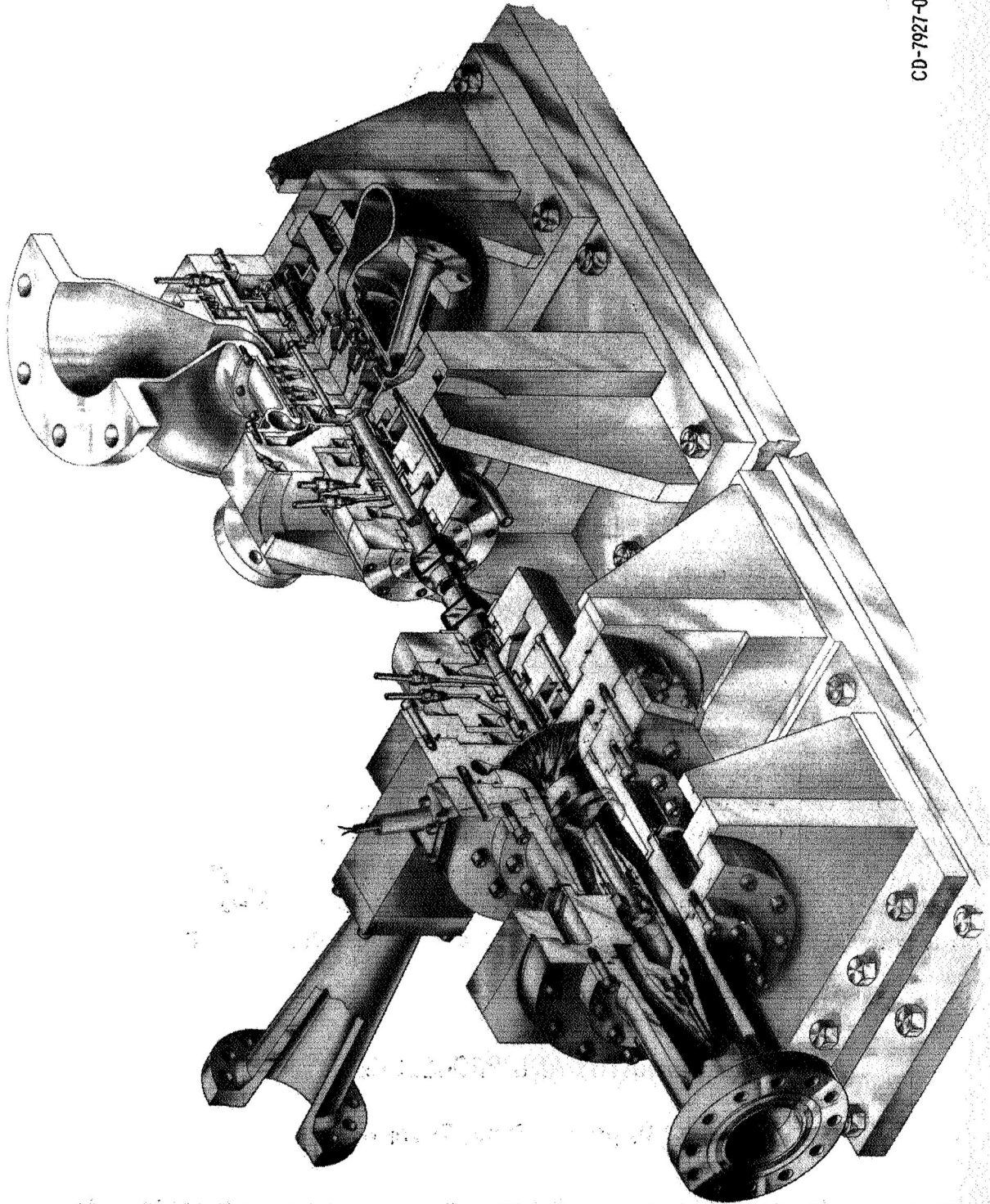
CD-7927-01

Figure 7. – Cross section of pump and turbine assembly.

8

was absorbed by a rotating balance disk operating in oil. A back-to-back seal arrangement, with gaseous helium between the seals, was used to isolate the thrust-balance oil from the liquid hydrogen. A similar thrust-balance and double-seal arrangement was used with the turbine assembly. The pump inducers and the impeller were machined from titanium. Under ambient conditions, the inducer radial tip clearance was set at 0.012 inch (0.030 cm), and the impeller tip-to-stationary shroud clearance was set at 0.014 inch (0.036 cm). The diffuser scroll assembly was machined and furnace brazed.

Test Facility

A schematic drawing of the test facility is shown in figure 8. Liquid hydrogen was pumped through an open-loop system from a 6000-gallon (22.7-cu m) supply Dewar to a 6000-gallon (22.7-cu m) receiver Dewar through a 3-inch- (7.62-cm-) diameter vacuum-jacketed stainless-steel pipe. The pump net positive suction pressure was controlled by regulation of the pressure in the supply Dewar. A venturi and flow control valve were located approximately 10 feet (3 m) downstream of the pump. The tests were remotely conducted from a building approximately 1/4 mile (400 m) from the test site.
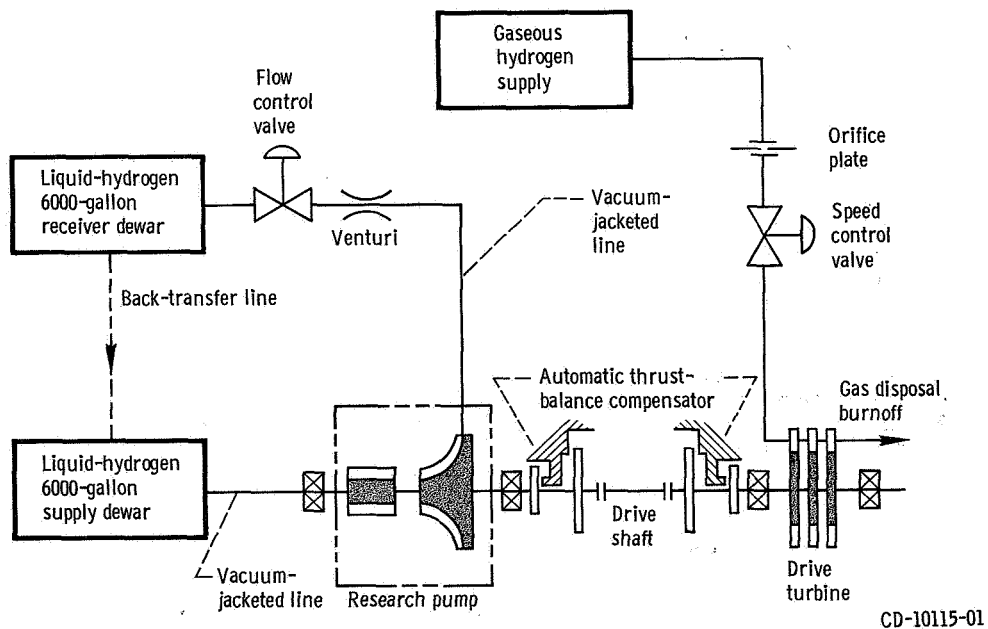
Figure 8. - High-speed liquid-hydrogen pump test facility.

9
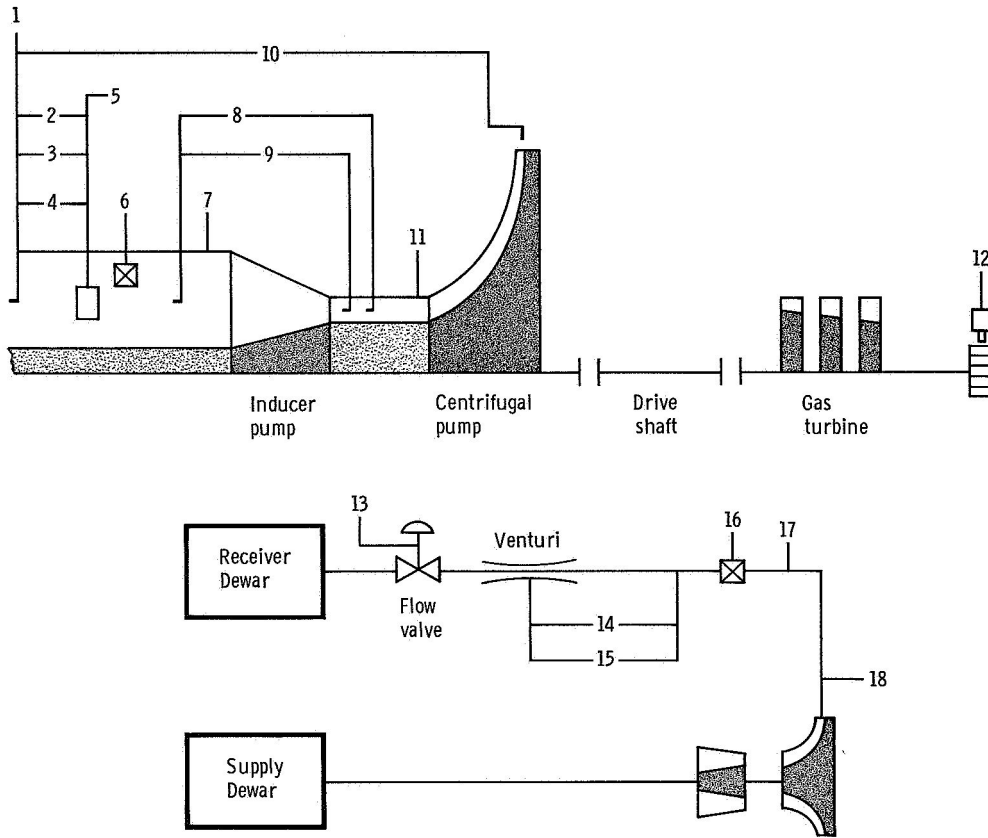
1. Inlet total pressure
2. Net-positive-suction-pressure range, 0 to 50 psi (0 to 34.5 N/cm^2)
3. Net-positive-suction-pressure range, 0 to 25 psi (0 to 25 psi (0 to 17.2 N/cm^2)
4. Net-positive-suction-pressure range, 0 to 5 psi (0 to 3.45 N/cm^2)
5. Vapor pressure (vapor bulb)
6. Inlet temperature (platinum resistor)
7. Inlet static pressure
8. Inducer pressure rise

9. Inducer pressure rise
10. Inducer and impeller pressure rise
11. Static pressure behind inducer
12. Speed indicator
13. Valve position
14. Flow rate range, 0 to 50 psi (0 to 34.5 N/cm^2)
15. Flow rate range, 0 to 25 psi (0 to 17.2 N/cm^2)
16. Outlet temperature (platinum resistor)
17. Outlet static pressure
18. High-frequency pressure transducer

CD-10116-01

Figure 9. – Instrumentation of liquid-hydrogen pump.

10

Instrumentation

A schematic drawing showing the location of the instrumentation in the test facility is shown in figure 9. The estimated instrumentation system accuracy is given in table III. Platinum resistors were used to measure liquid-hydrogen temperatures. Pump rotative speed was measured with a magnetic pickup in conjunction with a gear on the turbine drive shaft. Pump flow rate was obtained from a venturi flowmeter that was calibrated in both air and water. Pressures for evaluating the performance were measured with strain-gage transducers. Whenever possible, differential pressures were measured to allow smaller range pressure transducers to be used for greater accuracy. Net positive suction pressure was obtained directly with a differential pressure transducer in conjunction with a total pressure probe and a vapor bulb. All data were recorded on a high-speed digital potentiometer utilizing magnetic tape.

Test Procedure

All the tests were conducted in liquid hydrogen at a nominal fluid temperature of 37.0° R (20.6 K). For all test runs, speed and net positive suction pressure were held constant while the throttle valve position was automatically controlled with a ramp generator to provide a linear variation in flow. A severe pump vibration was encountered at approximately 42 000 rpm because of a critical speed of the rotative hardware. The rotational speed of the pump was therefore limited to 40 000 rpm.

Methods for Determining Unstable Flow

Two methods were used to determine unstable flow conditions. One method was employed during test operations, and the other was used for data analysis. The two methods are described in the following paragraphs.

During test operations, the unstable flow rate of the pump was determined by a high-frequency-response pressure transducer located in the pump outlet casing. The pressure signals from the transducer were recorded with a frequency-modulated data recording system with magnetic tape output. This system provides a continuous recording of a test parameter with a frequency response of 20 000 hertz. Data from the frequency-modulated recorder were monitored on an oscilloscope during the test runs. The test terminated when the high-frequency-response pressure signals showed an abrupt increase in pressure amplitude.

11

For data analysis purposes, the flow rate of the pump, at the initiation of unstable flow, was determined from an analysis of the data scatter recorded from the venturi flowmeter. A standard deviation was computed for the data scatter by using the equation presented in appendix B. In this method of analysis, a data reading is referred to as a single measured value. Data readings were recorded by a digital potentiometer at a rate of 125 per second. For each data point, 25 successive readings were averaged. The standard deviation was computed for the 25 data readings to measure the degree of scatter that is associated with the given data point. The flow rate at which the standard deviation took a sharp rise was considered the onset of unstable flow.

The use of the two methods to determine the unstable flow region is illustrated in figure 10 for a sample test run. Pressure, standard deviation in flow, and flow ratio Q/Q_{des} are plotted as a function of time from the start of the test run. In this particular run, the pump was operated at a constant rotative speed of 20 000 rpm and
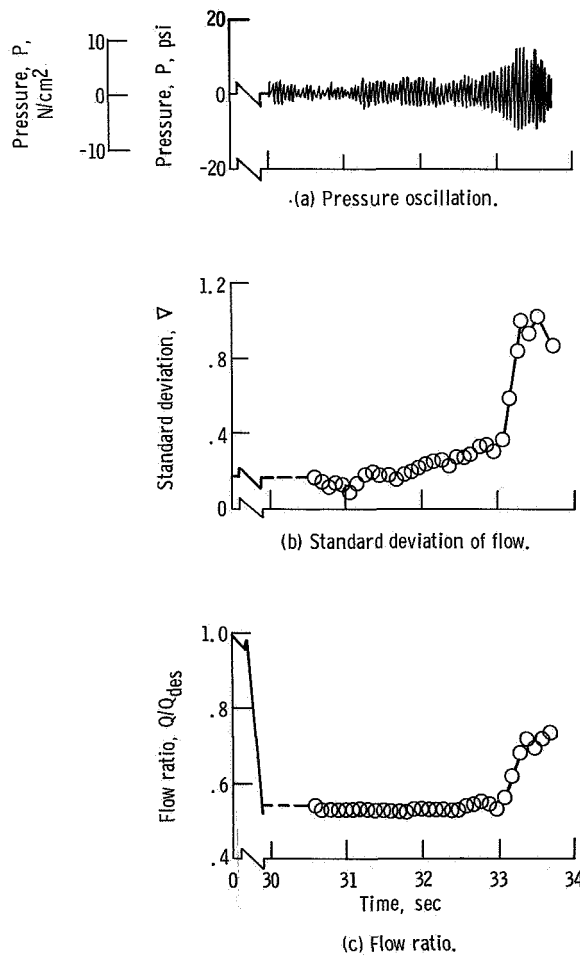

(a) Pressure oscillation.

(b) Standard deviation of flow.

(c) Flow ratio.

Figure 10. - Determination of unstable flow. Ramp rate, 5 gallons per minute per second (3.15x10^{-4} cu m/sec^2).

12

at a net positive suction pressure of 0.5 psi (0.35 N/cm^2). The flow was throttled at a constant rate of 5 gallons per minute (3.15×10^{-4} cu m/sec^2) throughout the test run. At 32.95 seconds, the pressure amplitude and standard deviation increased sharply, as shown in figures 10(a) and (b), respectively. The flow ratio, at the time when the pressure amplitude and standard deviation took a sharp increase, was 0.53 (fig. 10(c)), which was considered to be the initiation of unstable flow. The initiation of unstable flow also coincides with the increased amplitude of the high-frequency pressure signals monitored on the oscilloscope during the test runs.

RESULTS AND DISCUSSION

The overall pump performance of the three inducer-impeller combinations is shown in figure 11, where pump pressure rise is plotted as a function of flow rate. The performance was obtained at three values of net positive suction pressure, as noted in the figure, and at a pump rotational speed of 30 000 rpm. The pump design flow rate and pressure rise at this rotational speed were 550 gallons per minute (0.0347 cu m/sec) and 244 psi (168 N/cm^2), respectively. The measured pressure rise for the pump employing the 1.00-inducer at 550 gallons per minute (0.0347 cu m/sec) and 30 000 rpm was approximately 230 psi (158 N/cm^2). The suction specific speed computed at these conditions was 51 600.

For a comparison of pump performance between the three inducer-impeller configurations, the data obtained from the three configurations were combined and are presented in the next two sections. The results are plotted in terms of nondimensional parameters.

Noncavitating Overall Performance

The noncavitating performance for the three inducer-impeller configurations is presented in figure 12, in which the head coefficient ψ is plotted as a function of the flow ratio Q/Q_{des}, where Q_{des} is taken as the impeller design flow scaled to the particular test speed at which the data were obtained. The noncavitating performance is essentially identical for the three inducer-impeller configurations, all three producing a maximum head coefficient of approximately 0.70, which occurred at a flow ratio of approximately 0.8. This value compares with the design head coefficient of 0.72 and indicates that the efficiency was slightly lower than that assumed in the design and/or that the actual slip factor was less than the design value. Unstable flow, as indicated in the figure, occurred at a flow ratio of approximately 0.55 for all three configurations.

Net positive
suction pressure,
NPSP,
psi (N/cm^2)

○ 48 (33.1)
◇ 27 (18.6)
□ 1 (.7)

Solid symbols denote initiation
of unstable flow

Pump pressure rise, N/cm^2

Pump pressure rise, psi

320
240
160
80

200
150
100
50

Impeller
design
flow

200 300 400 500 600 700 800 900
Pump flow rate, Q, gal/min

.015 .020 .025 .030 .035 .040 .045 .050 .055
Pump flow rate, Q, cu m/sec

(a) 0.80-Inducer-impeller combination.

240
160
80
0

150
100
50

Impeller
design
flow

200 300 400 500 600 700 800 900
Pump flow rate, Q, gal/min

.015 .020 .025 .030 .035 .040 .045 .050 .055
Pump flow rate, Q, cu m/sec

(b) 1.00-Inducer-impeller combination.

240
160
80

150
100
50

Impeller
design
flow

200 300 400 500 600 700 800 900
Pump flow rate, Q, gal/min

.015 .020 .025 .030 .035 .040 .045 .050 .055
Pump flow rate, Q, cu m/sec
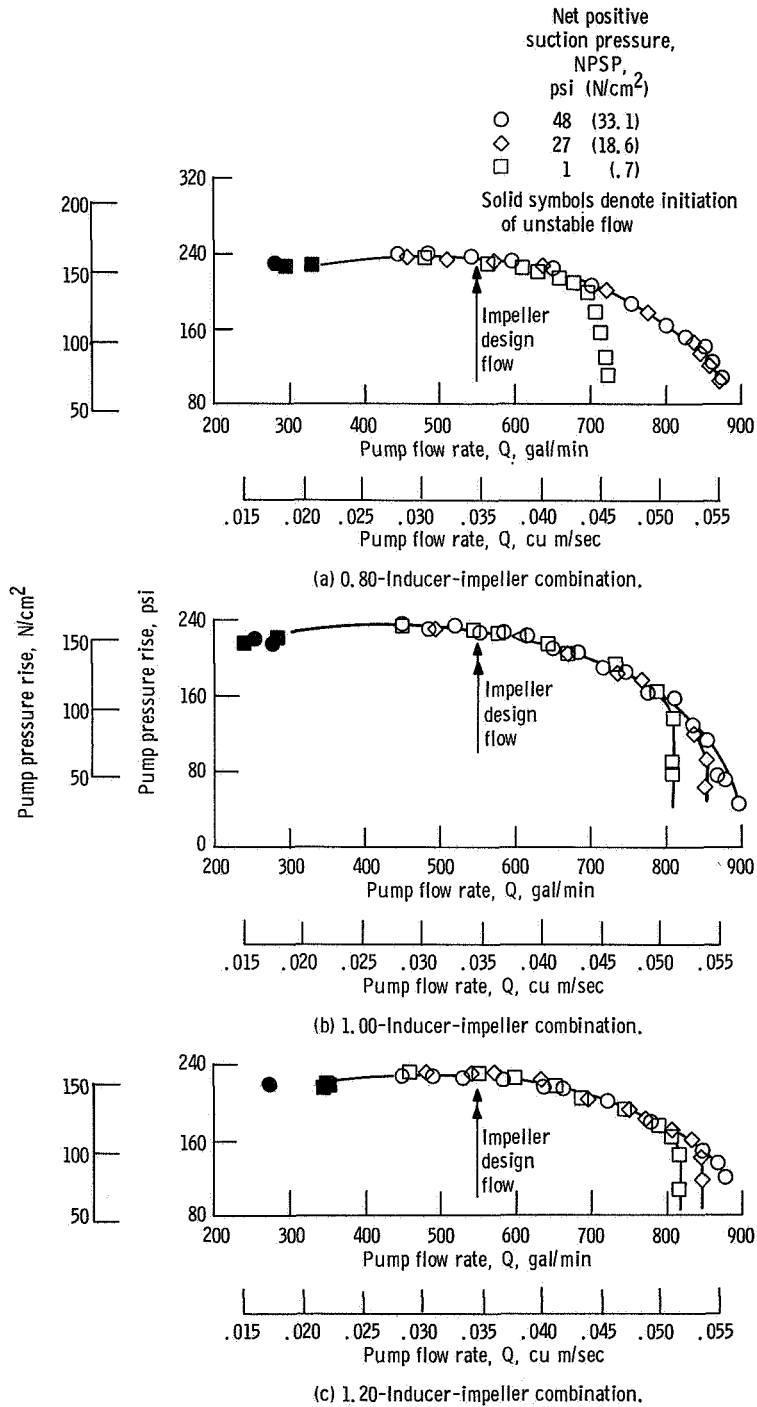
(c) 1.20-Inducer-impeller combination.

Figure 11. - Pump performance in liquid hydrogen at rotative
speed of 30 000 rpm.

14

Figure 12. - Overall noncavitating performance of three inducer-impeller combinations operating in liquid hydrogen.

From the point where unstable flow is indicated (solid symbols) to the point where the head coefficient is at a maximum, the performance curve has a positive slope. This characteristic is typical for a radial bladed centrifugal impeller, and when it is operating over this portion of the curve, the pump is vulnerable to system surge as discussed in the INTRODUCTION section.

The unstable flow points in figure 12 were obtained from the venturi flowmeter data by using the method of standard deviation of flow explained in the previous section. However, during the tests, pressure fluctuations attributed to system surge were visually evidenced from the output of the high-frequency-response pressure transducer. Pressure oscillations were observed as the pump flow rate was throttled along the positive-slope portion of the overall performance curve (fig. 10(a)). The amplitude of the pressure oscillations increased as the unstable flow condition, based on the standard deviation method, was approached.

Since the maximum head coefficient occurred at the same flow ratio for all three pump configurations, and the unstable flow point, determined by the standard deviation method, also occurred at essentially the same flow ratio, the inducer design flow appeared to have no effect on the point at which unstable flow occurred. It is doubtful, for an actual application, whether or not the performance on the positive slope is useful because of its susceptibility to system surge. The point of zero slope on the pump performance curve was not altered with the different inducer-impeller configurations. Thus, the minimum useful flow appeared to be unaffected as a result of the different inducer-impeller combinations.

The pump overall performance data presented in figure 12 were obtained at a rotative speed of 30 000 rpm. Superimposed on the curves in this figure are additional data points showing the point of unstable flow that was obtained at rotative speeds of 40 000 and 20 000 rpm. The initiation of unstable flow occurred at a nominal flow ratio of 0.55 over the range of rotational speeds and net positive suction pressures tested for the three inducer-impeller configurations. Thus, the point of initiation of unstable flow could be scaled with speed by use of the pump similarity laws.

Cavitating Overall Performance

The cavitating performance for the three inducer-impeller configurations is presented in figure 13. The portion of the curve between flow ratios of 0.65 and 1.10, instead of being faired through the data points, was reproduced from the noncavitating performance curve of figure 12. Similar to the noncavitating performance presented in the previous section, the initiation of unstable flow also occurred at a nominal flow ratio of 0.55 over the range of rotational speeds and net positive suction pressures tested.

As would be expected, the flow rate of the inducer-impeller combinations increased when the impeller was coupled with higher flow inducers, which provided more pressure to the impeller for the suppression of cavitation. The gain in the maximum obtainable flow was small between the 1.00-inducer-impeller and the 1.20-inducer-impeller. A comparison of the curves of the noncavitating with the cavitating head coefficient performance (figs. 12 and 13, respectively) for the three inducers shows that the cavitating performance for the 1.20-inducer-impeller approaches the noncavitating performance.

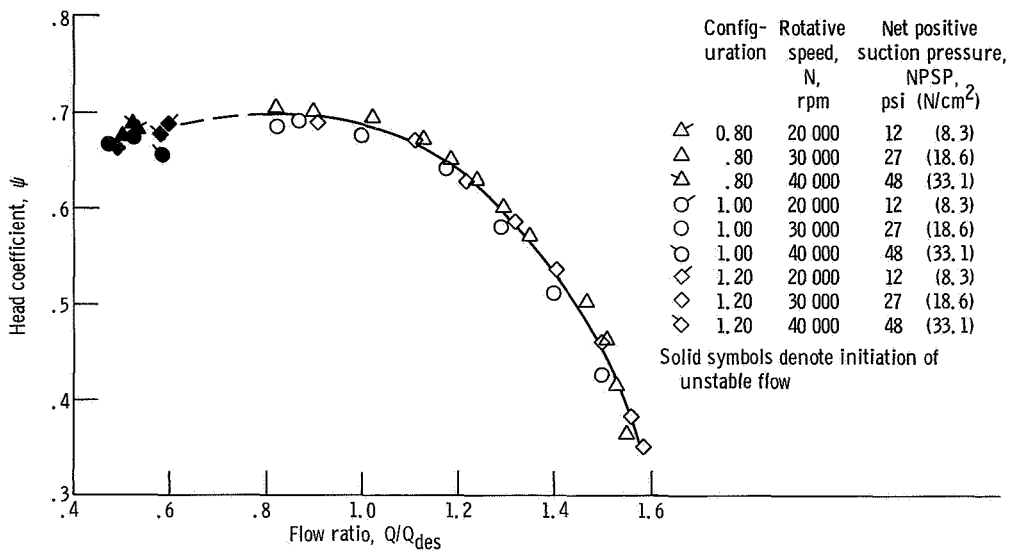| Config- uration	Rotative speed, N, rpm	Net positive suction pressure, NPSP, psi (N/cm^2)	
0.80	20 000	0.5	(0.35)
.80	30 000	1.0	(.70)
.80	40 000	2.0	(1.40)
1.00	20 000	.5	(.35)
1.00	30 000	1.0	(.70)
1.00	40 000	2.0	(1.40)
1.20	20 000	.5	(.35)
1.20	30 000	1.0	(.70)
1.20	40 000	2.0	(1.40)

Solid symbols denote initiation of unstable flow
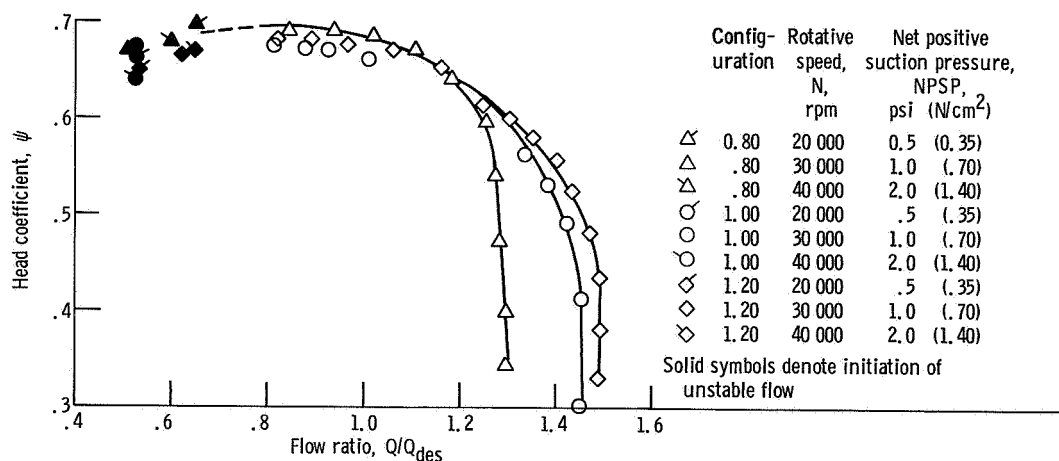
Figure 13. - Overall cavitating performance of three inducer-impeller combinations operating in liquid hydrogen.

16

High losses, at the higher flows, may be associated with the diffuser and scroll since they were designed for a flow ratio of 1.00 but were being operated at a flow ratio of 1.55. The noncavitating performance and possibly the cavitation performance of the 1.20-inducer would probably have been improved had the diffuser and scroll been designed for a higher flow ratio.

SUMMARY OF RESULTS

Three inducers were matched with one radial bladed centrifugal impeller. The inducers were designed to produce a given pressure rise at flow rates of 0.80, 1.00, and 1.20 of impeller design flow rate. The three inducer-impeller configurations were tested in liquid hydrogen. Analysis of the flow instabilities at low flow and the cavitation performance at high flows gave the following principal results:

1. The flow range of the inducer-impeller combinations was extended by designing the inducer for flow rates higher than the impeller design flow rate.

2. The flow ratio at which unstable flow occurred was essentially independent of inducer design flow. For the pumps used in this investigation, the initiation of unstable flow could be scaled with the pump rotative speed by the use of the pump similarity laws.

Lewis Research Center,
    National Aeronautics and Space Administration,
        Cleveland, Ohio, October 16, 1968,
            128-31-02-24-22.

APPENDIX A

SYMBOLS

g acceleration due to gravity, 32.17 ft/sec^2; 9.80 m/sec^2

ΔH head differential

k number of data readings

N rotative speed, rpm

P total pressure, psi; N/cm^2

ΔP pressure differential

p_v vapor pressure, psi; N/cm^2

Q flow rate, gal/min; cu m/sec

R radial coordinate, in.; cm

U rotor speed, ft/sec; cm/sec

V fluid velocity, ft/sec; cm/sec

W relative fluid velocity, ft/sec; cm/sec

Z axial coordinate, in,; cm

α slope of impeller hub, deg; rad

∇ standard deviation

θ impeller blade wrap angle, rad

λ data reading value

ρ density

φ flow coefficient

ψ head coefficient

Subscripts:

av   average

des   design

h   hub

i   inlet

n   initial value

s   shroud

t   tip

z   axial direction

18

APPENDIX B

EQUATIONS

Net positive suction pressure:

$$NPSP = P_i - p_v$$

Head-rise coefficient:

$$\psi = \frac{\Delta H}{\dfrac{U_t^2}{g}}$$

Flow coefficient:

$$\varphi = \frac{V_z}{U_t}$$

Flow ratio:

$$\frac{Q}{Q_{des}}$$

Head rise:

$$\Delta H = \frac{\Delta P \times 144}{\rho}$$

Standard deviation:

$$\nabla = \sqrt{\left[\frac{\sum\limits_{n=1}^{k} (\lambda_n)^2}{k} - (\lambda_{n,av})^2\right]\frac{k}{k-1}}$$

19

REFERENCES

1. Csanady, G. T.: Theory of Turbomachines. McGraw-Hill Book Co., Inc., 1964.

2. Ross, C. C.; and Banerian, Gordon: Some Aspects of High-Suction Specific-Speed Pump Inducers. Trans. ASME, vol. 78, Nov. 1956, pp. 1715-1721.

3. Stripling, L. B.: Cavitation in Turbopumps-Part 2. J. Basic Eng., vol. 84, no. 3, Sept. 1962, pp. 339-350.

4. Ball, Calvin L.; Meng, Phillip, R.; and Reid, Lonnie: Cavitation Performance of 84° Helical Pump Inducer Operating in 37° and 42° R Liquid Hydrogen. NASA TM X-1360, 1967.

5. Hamrick, Joseph T.; Ginsburg, Ambrose; and Osborn, Walter M.: Method of Analysis for Compressible Flow Through Mixed-Flow Centrifugal Impellers of Arbitrary Design. NACA Rep. 1082, 1952.

TABLE II. - IMPELLER BLADE CYLINDRICAL COORDINATES

(a) U.S. Customary Units

Slope of impeller hub, α, deg	Impeller blade wrap angle, θ, deg	Hub		Shroud		Number of blades
		Axial coordinate, Z_h, in.	Radial coordinate, R_h, in.	Axial coordinate, Z_s, in.	Radial coordinate, R_s, in.	
0	0	0	0.936	-----	-----	12
10	-15.993	.208	.954	0.143	1.326	
20	-27.101	.410	1.008	.295	1.326	
30	-35.603	.600	1.097	.460	1.340	
40	-42.173	.771	1.217	.620	1.397	24
50	-47.171	.919	1.365	.764	1.495	24
60	-50.829	1.039	1.536	.886	1.625	48
70	-53.307	1.128	1.726	.981	1.779	
80	-54.728	1.182	1.969	1.058	1.987	
90	-55.186	1.200	2.136	1.086	2.136	

(b) SI Units

Slope of impeller hub, α, rad	Impeller blade wrap angle, θ, rad	Hub		Shroud		Number of blades
		Axial coordinate, Z_h, cm	Radial coordinate, R_h, cm	Axial coordinate, Z_s, cm	Radial coordinate, R_s, cm	
0	0	0	2.377	-----	-----	12
.175	-.279	.528	2.423	0.363	3.368	
.349	-.473	1.041	2.560	.749	3.368	
.524	-.621	1.524	2.786	1.168	3.404	
.698	-.736	1.958	3.091	1.575	3.548	24
.873	-.823	2.334	3.467	1.941	3.797	24
1.047	-.887	2.639	3.901	2.250	4.128	48
1.222	-.930	2.865	4.384	2.492	4.519	
1.396	-.955	3.002	5.001	2.687	5.047	
1.571	-.963	3.048	5.425	2.758	5.425	

TABLE III. - ESTIMATED MAXIMUM INSTRUMENT SYSTEM ERRORS

(a) U.S. Customary Units

Inlet temperature, ^{o}R	
Pump	±0. 15
Venturi	±0. 15
Pressure rise, psi	
Inducer	±0. 10
Inducer-impeller pump	±5. 0
Net positive suction pressure, NPSP, psi	
Low range	±0. 05
Midrange	±0. 25
High range	±0. 50
Venturi differential pressure, ΔP, psi	
Low range	±0. 25
High range	±0. 50
Rotative speed, N, rpm	±100

(b) SI Units

Inlet temperature, K	
Pump	±0. 083
Venturi	±0. 083
Pressure rise, N/cm^2	
Inducer	±0. 069
Inducer-impeller pump	±3. 45
Net positive suction pressure, NPSP, N/cm^2	
Low range	±0. 035
Midrange	±0. 172
High range	±0. 35
Venturi differential pressure, ΔP, N/cm^2	
Low range	±0. 172
High range	±0. 35
Rotative speed, N, rpm	±100

"The aeronautical and space activities of the United States shall be
conducted so as to contribute . . . to the expansion of human knowl-
edge of phenomena in the atmosphere and space. The Administration
shall provide for the widest practicable and appropriate dissemination
of information concerning its activities and the results thereof."

— National Aeronautics and Space Act of 1958

NASA SCIENTIFIC AND TECHNICAL PUBLICATIONS

TECHNICAL REPORTS: Scientific and
technical information considered important,
complete, and a lasting contribution to existing
knowledge.

TECHNICAL NOTES: Information less broad
in scope but nevertheless of importance as a
contribution to existing knowledge.

TECHNICAL MEMORANDUMS:
Information receiving limited distribution
because of preliminary data, security classifica-
tion, or other reasons.

CONTRACTOR REPORTS: Scientific and
technical information generated under a NASA
contract or grant and considered an important
contribution to existing knowledge.

TECHNICAL TRANSLATIONS: Information
published in a foreign language considered
to merit NASA distribution in English.

SPECIAL PUBLICATIONS: Information
derived from or of value to NASA activities.
Publications include conference proceedings,
monographs, data compilations, handbooks,
sourcebooks, and special bibliographies.

TECHNOLOGY UTILIZATION
PUBLICATIONS: Information on technology
used by NASA that may be of particular
interest in commercial and other non-aerospace
applications. Publications include Tech Briefs,
Technology Utilization Reports and Notes,
and Technology Surveys.

Details on the availability of these publications may be obtained from:

SCIENTIFIC AND TECHNICAL INFORMATION DIVISION

NATIONAL AERONAUTICS AND SPACE ADMINISTRATION
Washington, D.C. 20546